Applied Surface Science 323 (2014) 45–53

Applied Surface Science

journal homepage: www.elsevier.com/locate/apsusc

# Ambient pressure photoemission spectroscopy of metal surfaces

Iain D. Baikie*, Angela C. Grain, James Sutherland, Jamie Law

*KP Technology Ltd, 12 A Burn Street, Wick KW1 5EH, Caithness, UK*

ARTICLE INFO

*Article history:*
Received 1 May 2014
Received in revised form 24 August 2014
Accepted 26 August 2014
Available online 3 September 2014

*Keywords:*
Photoemission Spectroscopy
SPV
SPS
Metal oxides
Work function
$Cu_2O$

ABSTRACT

We describe a novel photoemission technique utilizing a traditional Kelvin probe as a detector of electrons/atmospheric ions ejected from metallic surfaces (Au, Ag, Cu, Fe, Ni, Ti, Zn, Al) illuminated by a deep ultra-violet (DUV) source under ambient pressure. To surmount the limitation of electron scattering in air the incident photon energy is rastered rather than applying a variable retarding electric field as is used with UPS. This arrangement can be applied in several operational modes: using the DUV source to determine the photoemission threshold ($\Phi$) with 30–50 meV resolution and also the Kelvin probe, under dark conditions, to measure contact potential difference (CPD) between the Kelvin probe tip and the metallic sample with an accuracy of 1–3 meV. We have studied the relationship between the photoelectric threshold and CPD of metal surfaces cleaned in ambient conditions. Inclusion of a second spectroscopic visible source was used to confirm a semiconducting oxide, possibly $Cu_2O$, via surface photovoltage measurements with the KP. This dual detection system can be easily extended to controlled gas conditions, relative humidity control and sample heating/cooling.



## 1. Introduction

The traditional Kelvin probe (KP) [1] equipped with a macroscopic tip is a versatile tool for measuring, in a non-contact fashion, exquisitely small differences in work function ($\Delta\Phi$, $\Delta E_f$) or contact potential (CPD) between a vibrating metallic reference electrode and a metallic or semiconducting sample. Traditionally the Kelvin method has been applied for in-situ characterization of metals and semiconductors [2–5]. More recently it has been utilized in studies under ambient conditions of organic semiconductors: surface photovoltage characterization of bulk heterojunction organic solar cells [6]; *p*-type doping of P3HT with $F_4$TCNQ [7] and $\Phi$-tuning of graphene [8] and ITO [9].

CPD is essentially a difference method, to calculate absolute sample $\Phi$ data assumptions are required on $\Phi_{tip}$ and its stability under experimental conditions. Both assumptions are potentially sources of experimental error. Baikie et al. [10] have described a UHV calibration method using a Hg lamp as a UV light source and a low-$\Phi$ sample in a retarding field configuration to the KP tip. Previous studies of metals [11] and ITO [12] have been performed using a combination of vacuum UPS measurements (absolute $\Phi$) and CPD. However, these studies involve *separate* UHV photoemission (PE) and ambient pressure CPD measurements. The underlying assumptions are (a) that ambient samples remain unaffected by the vacuum conditions and (b) samples generated in vacuum remain stable after exposure to ambient gases such as $O_2$ and $H_2O$.

In this paper we report, for the first time, a combination of ambient pressure photoemission spectroscopy and CPD using a 2 mm diameter Kelvin probe. In both measurements the *same tip electrode* is used as the current collector and the two measurements can be conducted quasi-simultaneously. An advantage of this new procedure is that $\Phi_{sample}$ is determined independent of $\Phi_{tip}$.

This method can readily extended to semiconductor surfaces to include surface photovoltage spectroscopy (SPV), providing information on non-neutral surface space-charge regions (SCR) [13]. An advantage of this arrangement is that this arrangement technique can characterize $\Phi$, $E_f$, and surface potential $V_s$, allowing monitoring of changes in energy barriers within electronic layers and devices as a function of exposure to ambient conditions, for instance diffusion of $O_2$, $H_2O$. The metals described in this study are in general use as anode/cathodes in solar cells or in the case of copper oxide as a photon absorber.

### 1.1. Experimental methods 1: CPD/SPV

The CPD generated by vibrating metallic tip in proximity to a dissimilar metal surface is equal to their difference in work function, i.e. $eV_{cpd} = e(\Phi_{KP} - \Phi_M)$ see Fig. 1. When electrical contact is

* Corresponding author. Tel.: +44 01955602777.
*E-mail addresses:* iain@kptechnology.ltd.uk, BaikieUK@Hotmail.co.uk (I.D. Baikie).

http://dx.doi.org/10.1016/j.apsusc.2014.08.159

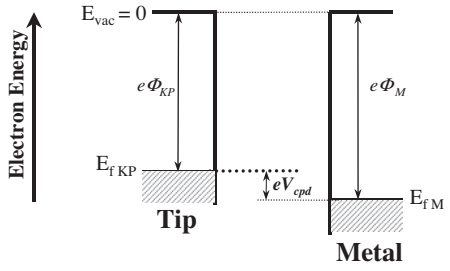


**Fig. 1.** Electron energy diagram for a metallic Kelvin probe tip of work function $\Phi_{KP}$ and dissimilar metal sample of work function $\Phi_M$. The energy difference between the two Fermi-levels is equal to $eV_{cpd}$, i.e. $eV_{cpd} = (Ef_{KP} - Ef_{KM})$. $E_{vac}$ represents the vacuum level.

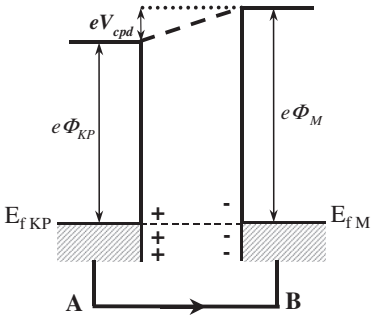


**Fig. 2.** Upon electrical contact the metal Fermi-levels equalize via a transfer of electrons from the lower work function tip to the metal sample. This results in a positively charged tip and a negatively charge sample and an associated electric field between the two adjacent surfaces. If an external emf, termed $V_b$ is included between points AB then, when $V_b = -V_{cpd}$, the surface charges vanish and a null field exists between KP tip and sample.

made between the two metals charge flows from the lower work function to the higher, resulting in a negatively charged high work function surface and a positively charged low work function surface. An electric field now exists between the two metals, see Fig. 2. If an externally controlled emf, termed the backing potential $V_b$, is inserted between points A and B in Fig. 2, then the relative position of the metal sample Fermi-level can be altered. When the Kelvin probe tip is vibrated to produce a modulated capacity, then the peak-to-peak output $V_{ptp}$ will be proportional to $(V_b - V_{cpd})$. At the unique point where, $V_b = V_{cpd}$ the surface charges disappear and the electric field between tip and sample is zero (or null).

Unfortunately the null position coincides with a minimum in the signal to noise (S/N) ratio, consequently all null-field Kelvin probes are liable to errors resulting from laboratory noise, stray capacity and overtalk from the probe vibration frequency and its harmonics. The off-null detection method described by Baikie [1] alleviates these issues by employing a current-sensitive approach preserving a high signal level. Further tip-to-sample capacity information can be used to minimize the environmental stray capacity effect and allow sub-micron tip-to-sample positioning. Fig. 3 illustrates this method: assuming the tip potential is changed from $Vb_1$ to $Vb_2$ then the output signal changes from $Vptp_1$ to $Vptp_2$. The null position can be calculated with 1–3 meV resolution from two high signal level measurements and the gradient M of the $\Delta V_{ptp}/\Delta V_b$ line can be used in a feedback control loop to maintain a mean tip-to-sample distance aiding initial approach, repeatability and scanning.

The Kelvin probe used in this study utilizes a 2.0 mm diameter tip with a gold alloy coating. It was operated at 70 Hz and the tip-to-sample mean spacing was approximately 1.0 mm with a PTP vibration amplitude of 0.460 mm. The Kelvin probe is located in a Faraday cage allowing the sample illumination to be controlled.

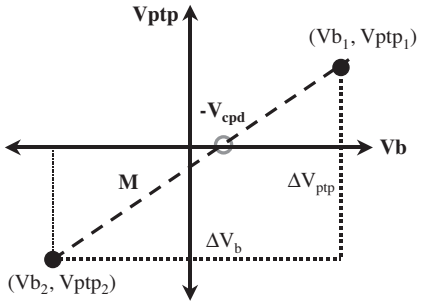


**Fig. 3.** If the tip is now vibrated then the peak-to-peak height of the resulting waveform is proportional to $(V_{cpd} - V_b)$ and the grey circle above represents the balance position. The minimum S/N ratio at null can be avoided by making two or more ($V_{ptp}$, $V_b$) measurements and then extrapolating. The gradient M of the extrapolated line is proportional to the fractional capacity [1] and can be used in a feedback circuit to maintain the tip-to-sample mean spacing.

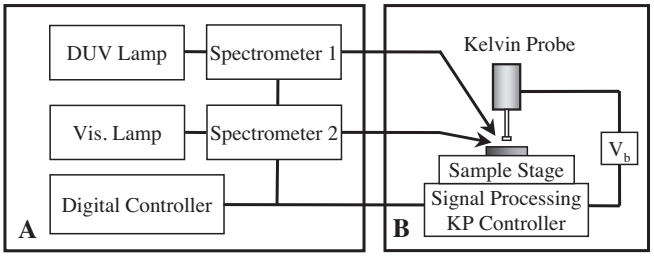


**Fig. 4.** Schematic diagram of the ambient photoemission spectroscopy system: (A) DUV lamp ($D_2$), motorized spectrometer and DUV optical filter arrangement produce a tuneable 3.0–7.0 eV beam. The DUV spectrometer enclosure is filled with $N_2$ to eliminate ozone production. The QTH lamp and visible spectrometer is used for surface photovoltage measurements. (B) Faraday Cage/Light Chamber with vertically mounted Kelvin probe which is used as a current detection in both photoemission and CPD measurement modes. $V_b$ is the tip bias potential. The sample is mounted on a 3-axis stage with optional heater/cooler. The chamber can optionally be relative humidity controlled.

The sample was located on a motorized $(x,y,z)$ sample stage with transitional position control <300 nm.

A second optical source, using a quartz Tungsten–Halogen lamp and associated spectrometer, permits sample illumination with either controllable intense white light or variable wavelength 400–1000 nm ($E_{ph}$: 3.1–1.24 eV) irradiation. This system can be used to test for formation of a semiconducting surface via changes in surface potential $V_s$ due to illumination by a intensity modulated white light source or by scanning the wavelength above and below the band-gap energy $E_g$ [13].

### *1.2. Experimental methods 2: Ambient pressure photoemission spectroscopy*

The ambient pressure photoemission system comprises a deuterium ($D_2$) source coupled with a motorized grating monochromator. The sample is illuminated via a DUV optical fibre resulting in an elliptical surface profile of approx. 3 × 4 mm. Nitrogen gas is used to suppress the production of ozone in the DUV spectrometer. The range of incident $E_{ph}$ is typically 3.0–7.0 eV, see Fig. 4. The photoelectron emission and ion-current detection process is a 4-step process, illustrated in Fig. 5:

1. DUV photons are absorbed within the metal surface region. Provided $E_{ph} \geq \phi_m$ electrons within the range of the inelastic electron mean free path (escape depth) of electron excitation can be emitted. The electron escape depth as a function of electron energy describes a U-shaped curve with a minimum depth of circa 0.5 nm between 50–100 eV [14]. In our case, with photon

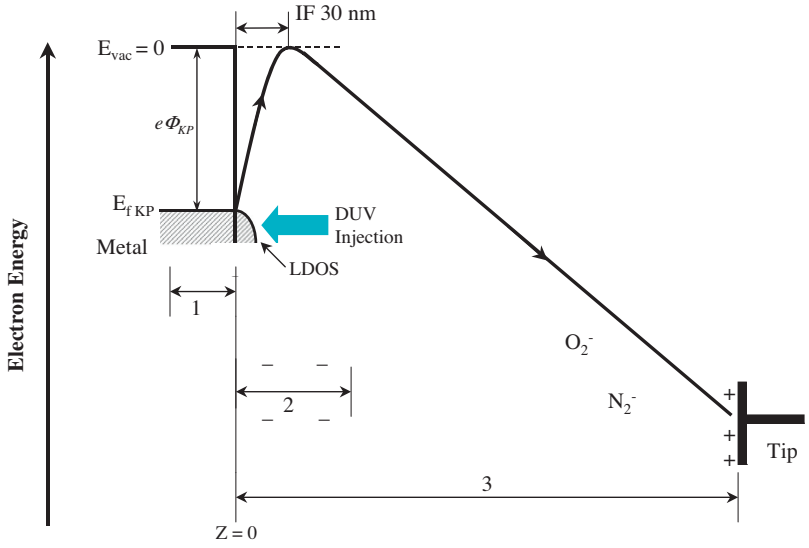


**Fig. 5.** Schematic energy band diagram (not to scale) representing the processes involved in ambient pressure photoemission. (1) Injection of DUV photons. LDOS represents the local density of states and "IF" the circa 30 nm range of the image force. (2) Photoejected electrons form an electron cloud in the region 1–3 um from the metal surface ($Z = 0$) producing atmospheric ions. Electron kinetic energy information is lost due to scattering but charge continuity is preserved. (3) Ions drift toward the positively biased (+10 V) Kelvin probe tip under a modest electric field. No significant surface barrier lowering occurs.

energies close to $E_f$, electronic scatting within the metal is relatively low. After exiting the metal photoejected electrons are subject to the image force (IF) between the electron and the positively charged metal. The IF extends to approximately 30 nm from the metal surface, beyond this range the electrons are subject to (a) scattering by atmospheric molecules and (b) external electric fields.

2. An electron cloud is formed immediately outside the metal. Under ambient conditions the mfp of the elected electrons is typically 1–3 um. Inelastic scattering by the much more massive $N_2$, $O_2$ and $H_2O$ molecules means that the electron's kinetic energy information is lost, however the electron charge is preserved. In this region atmospheric ions such as $N_2^-$ and $O_2^-$ and possibly $OH^-$ are generated.
3. Charged atmospheric ions drift towards the positively biased Kelvin probe tip. The field gradient is rather modest, circa 10 V/mm consequently there is no field-induced barrier height lowering or electron tunnelling contribution from electrons across the barrier, i.e. the absolute work function is involved, unlike the case with "local" AFM and STM probes.
4. The ion current is recorded as a function of incident photon energy. Below the work function threshold energy no emission occurs and above the threshold the ion current will increase with $(E_{ph} - \Phi_M)^{1/2}$ [15]. We expect this method to provide information about states within 1–3 eV of $E_f$ and thus be sensitive to changes in the local density of states (LDOS).

In our configuration the DUV light illuminates the sample, the rear surface of the gold-alloy tip and the front surface of the tip via reflection from the sample. The tip is maintained at a positive bias of +10 V. This positive bias serves two functions: to attract the photoelectrons/ion from the sample and secondly to re-attract any photoelectrons/ions emitted by the tip itself. At the potential used (+10 V) we cannot detect any emission from the tip when the sample is well removed, e.g. to a distance 2 cm below the tip.

The $D_2$ maximum photon energy (7.3 eV) is much smaller than the 21.1 and 40.8 eV primary energies used in UPS (He source). However $E_{ph}$ range matches the photoelectric threshold of many metals and semiconductors and the low photon energy is much less likely to damage the surface or produce unwanted surface charging. The detection system in CPD/SPV or APS modes of operation is capable of current measurement in the range of 0.1 fA–100 nA.

## 2. Materials

Photoelectron spectroscopy and CPD measurements were performed under ambient conditions on a set of sheet and foil metallic samples (Fe 99.7%, Ag 99.998%, Al 99.99% Newmet Koch; Au (99.985%), Ti 99.7%, Zn 99% Alfa Aesar, Cu 99.998% Sigma–Aldrich, HOPG (SPI-1, SPI) was included in the sample set as its clean surface can be readily generated. Samples of Fe, Zn, Ti and Cu were prepared using IPA and polishing with 1 μm diamond paper; the others were measured as received. Sample mounting and alignment took under 60 s, as the KP tip approach is an automatic procedure resulting in all measurements being conducted at the same tip-to-sample distance (with 1 μm resolution). The CPD was recorded and averaged over 1 min and the PE data spectra were acquired over a further 4–10 min. The Relative humidity during these measurements was (38 ± 3)% and the temperature (20 ± 2)°C.

## 3. Results and discussion

### 3.1. Normalized intensity corrected photoresponse

Normalized intensity-corrected photoemission spectra for four metals (Ag, Au, Cu and Al) are shown in Fig. 6 for energies of circa 3.5–7.0 eV (350–177) nm with 1 nm increments. Cu and Al surfaces have been mechanically polished and Ag and Au are as-received. We should stress that there is no suggestion that these surfaces are atomically clean, i.e. we would anticipate that, even after mechanically cleaning, Cu and Al surfaces are likely to be partially oxidized. Ag forms a sulphide $Ag_2S$ in ambient, whereas Au, and indeed all the metals, will also have adhering layers of weakly adsorbed water vapour.

We observe that these metals display high signal levels: Al displays the best photoresponse followed by Cu, Ag and Au. Al clearly displays the lowest photoelectric threshold—the other metals are difficult to separate in this plot. The photoresponse curve of Al exhibits a shoulder approximately 0.8 eV above the

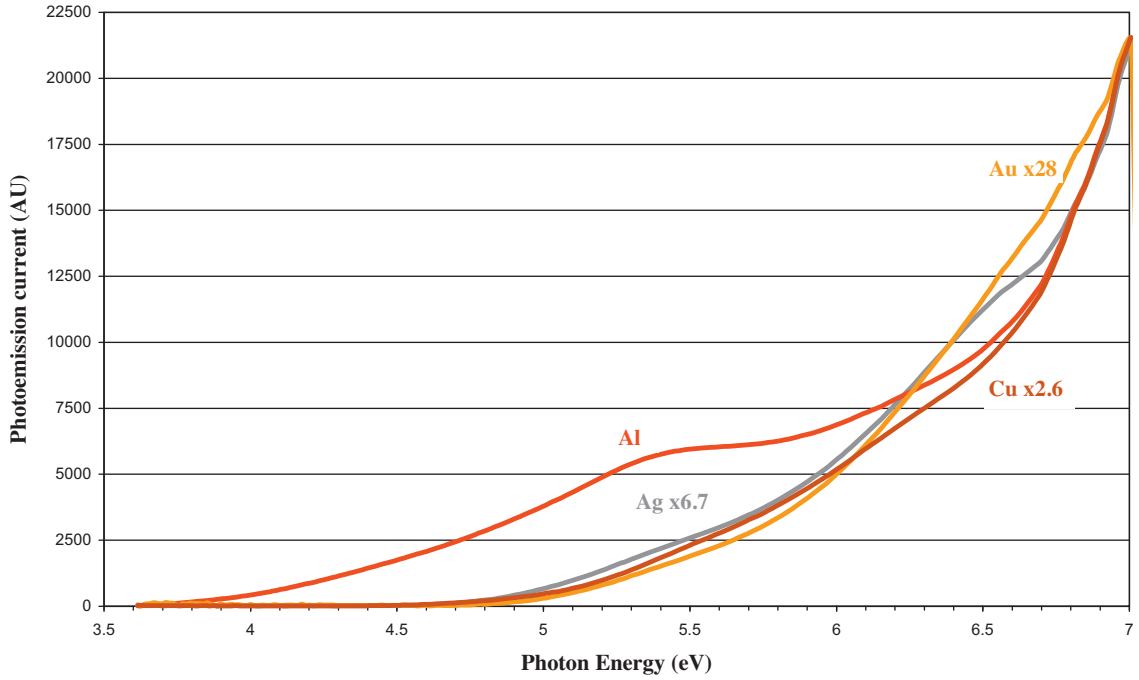


**Fig. 6.** Plot of intensity corrected normalized photoemission response of Al, Cu, Ag and Au clean metal surfaces at ambient pressure over the photon energy range 3.5–7.0 eV. The zero-offset of each metal have been adjusted to coincide.

initial photoelectric threshold and a smaller feature appears for Ag, approximately 1.0 eV above threshold.

### 3.2. Square root photoresponse: Fowler Theory

We are interested in determining whether electrons can readily be transported through such surface layers and if the resulting spectra can be easily interpreted in terms of the Fowler Theory [15], where $R \propto (E_{ph} - h\upsilon_o)^2$ where $R$ is the photocurrent per adsorbed photon, $E_{ph}$ the photon energy, $h$ is Planck's constant and $\upsilon_o$ the threshold frequency. We thus anticipate a linear relationship when the square root of the photoresponse is plotted as a function of photon energy, i.e. $R^{1/2} = k(E_{ph} - h\upsilon_o)$.

In a first analysis we may expect $h\upsilon_o$ to represent the metal work function $\Phi_M$, however, it remains to be seen if these samples exhibit a homogeneous work function or are dominated by local geometric effects induced by polishing or surface contamination. Crowell et al. [16] showed that for W–Si and WGaAs diodes the photoresponse is linear for Eph approximately 0.1 eV above the photoelectron threshold, with the barrier height (i.e. difference in Fermi-level between metal and semiconductor). In this study we consider, as a first analysis, the fit of the initial photoelectric threshold.

### 3.3. Square root photoresponse data

The square-root photoresponse data for Ag, Au, Cu and Al are shown in Figs. 7–10, respectively. In each figure we have determined the initial photoelectric threshold using linear extrapolation of the straight-line section and computing the interception with the zero baseline. We also report other extrapolations from any other straight-segments occurring at higher energies. We have several reasons reason for such analysis:

1. We cannot be certain that the initial photoelectron threshold is indeed the metal work function $\Phi$, it could be due to contamination, physisorbed or adsorbed atmospheric components, or geometric features (field emitter tip).
2. We cannot assume that surface layers or films, such as oxides, will necessarily obey Fowler Theory.
3. Calculated photoelectric thresholds are the intersection of the straight-line section with the zero-baseline which represents the detection system noise level. Thus if the noise level increases then the determination of the intersection becomes less exact producing a bias towards elevated threshold energies.

For Ag we observe an initial photemission threshold at 4.59 eV based upon a 0.7 eV linear extrapolation between 4.7 and 5.4 eV. A second intercept at 4.89 eV is generated from a straight-line segment commencing at 5.9 eV. Au also displays two values at 4.80 and 5.11 eV, for Cu 4.45 eV and 4.65 eV. Al display's only one threshold at 3.56 eV. In Fig. 11 we have plotted the measured CPD in darkness for Al, Zn, Ti, Ni, Fe, Cu, Ag, Au and HOPG versus the photoemission threshold.

We observe that the data fit reasonably well to a straight line ($R^2 = 0.982$) of gradient 1.085. Ideally the gradient would equal unity as for metals $\Delta V_{cpd} = \Delta\Phi$. The absolute work function of the Kelvin probe tip ($\Phi_{KP} = 4.764$ eV) is determined by the intercept with the line $V_{cpd} = 0$. We acknowledge that all photoemision techniques are sensitive to the lowest $\Phi$ patch of the $3 \times 4\,mm^2$ irradiated surface, whereas the CPD measurements are the area-averaged $\Phi$ (underneath the 2 mm diameter tip).

Table 1 shows the initial photoemission threshold values, together with selected values from the literature [17–20], and the dark CPD value. We observe that the data reported are generally in good agreement with literature; however, we note that literature values can span a wide range. For instance 5.10 eV is a commonly reported value for $\Phi_{Au}$ [21]. We note that the intercept of the 5.9–7.0 eV data for Au is 5.11 eV, see Fig. 8. We speculate that variations in $\Phi$ literature data could arise via intercepts of different sections of the photoresponse curve with the baseline, which may be affected by the detection method, prevailing S/N ratio material condition, etc. Further experimental work, conducted under

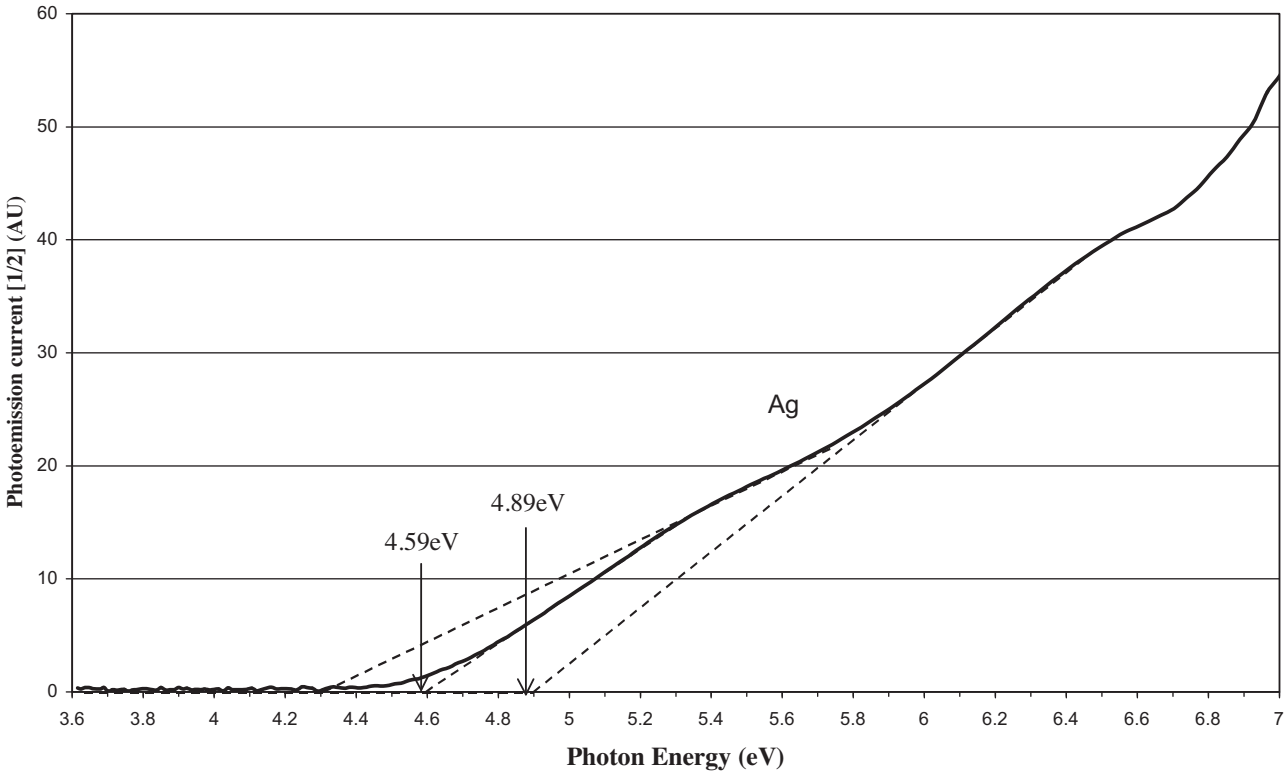


**Fig. 7.** Square root photoemission data for Silver. Extrapolation of the linear segments gives an initial photoemission threshold of 4.59 eV (4.6–5.3 eV extrapolation) and another at 4.89 eV (5.9–6.5 eV extrapolation).

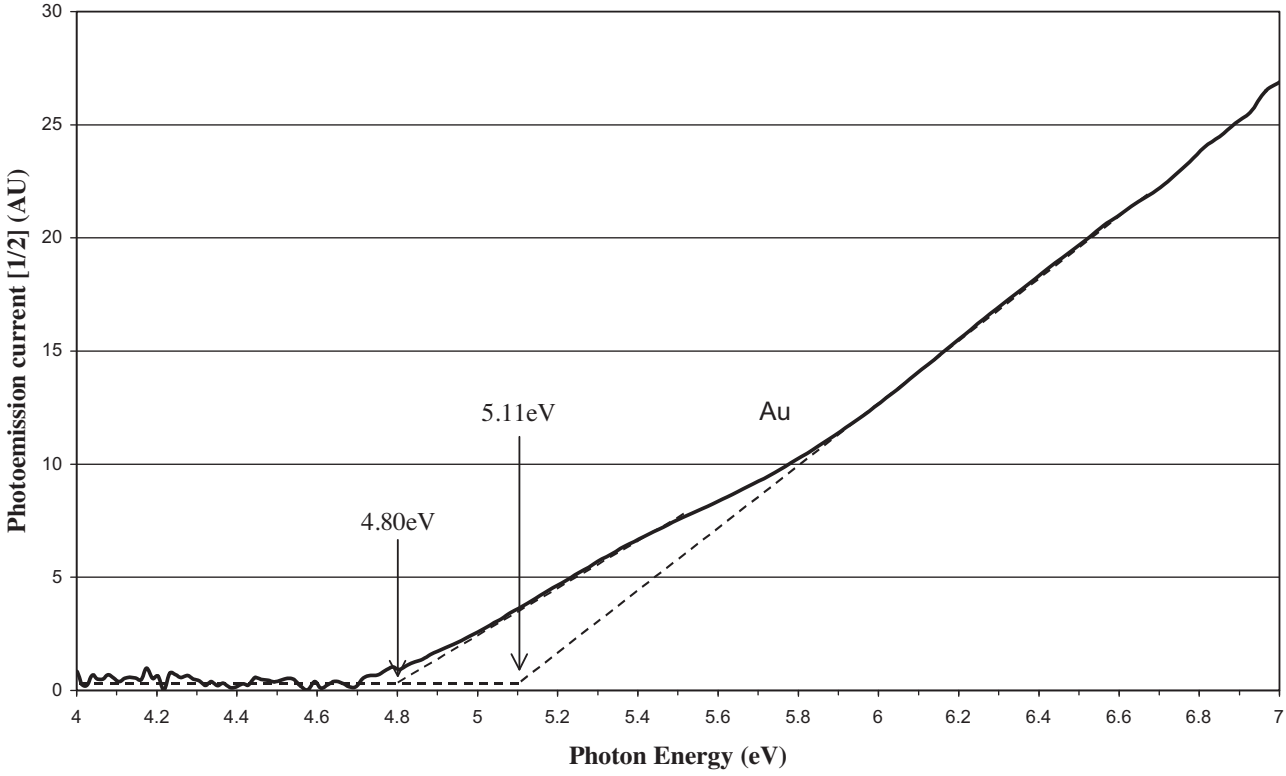


**Fig. 8.** Square root photoemission data for gold foil. Extrapolation of the linear segments gives an initial photoemission threshold of 4.80 eV (4.9–5.4 eV extrapolation) and another at 5.11 eV (5.9–7.0 eV extrapolation).

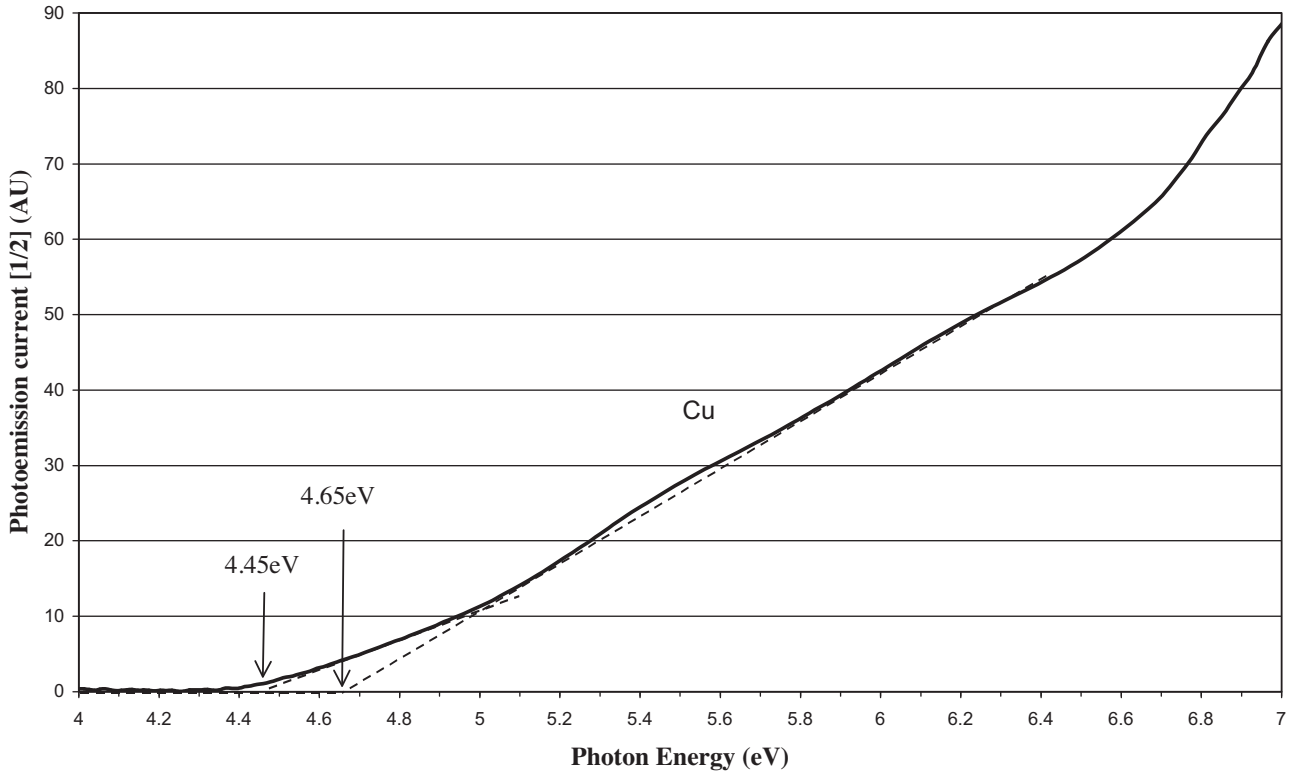


**Fig. 9.** Square root photoemission data for Cu. Extrapolation of the linear segments gives an initial photoelectric threshold of 4.45 eV (4.5–5.0 eV extrapolation) and 4.65 eV (4.9–6.5 eV extrapolation).

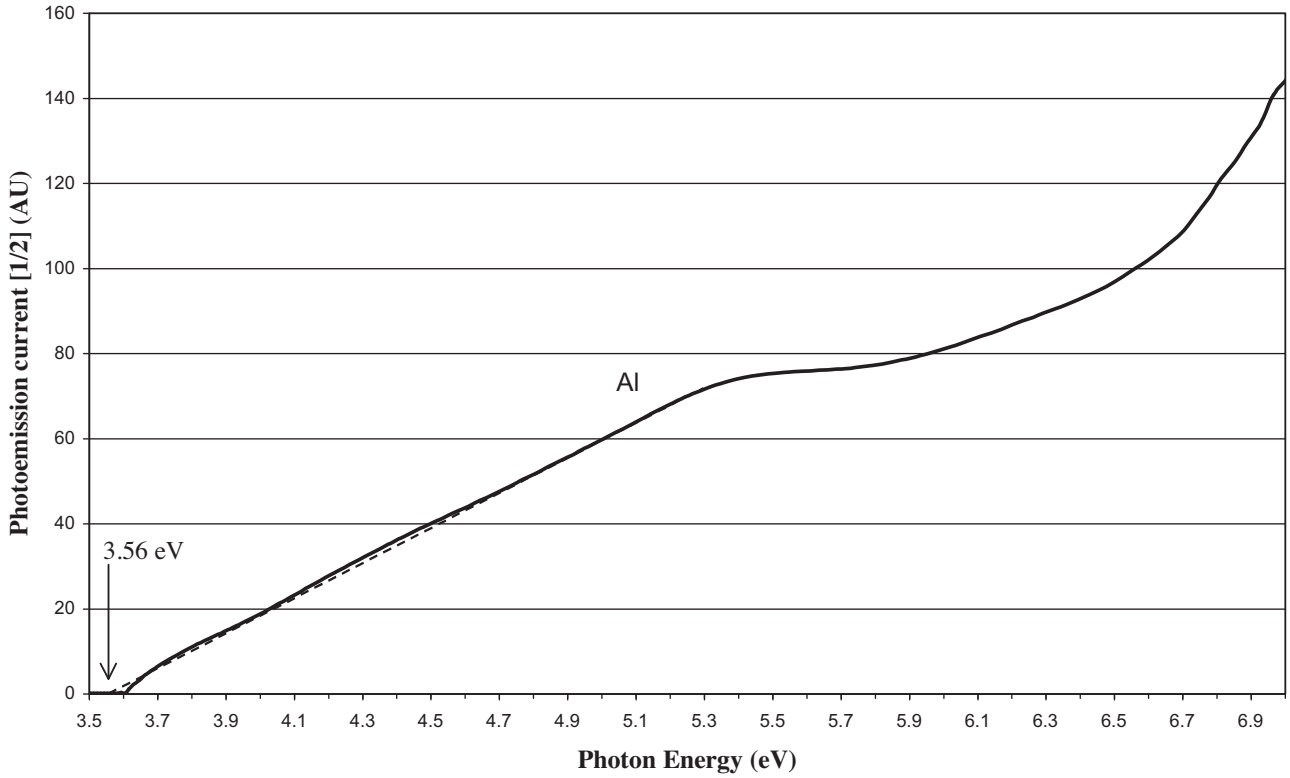


**Fig. 10.** Square root photoemission data for aluminium. Extrapolation of the linear segment gives a photoemission threshold of 3.56 eV (3.7–5.3 eV extrapolation).

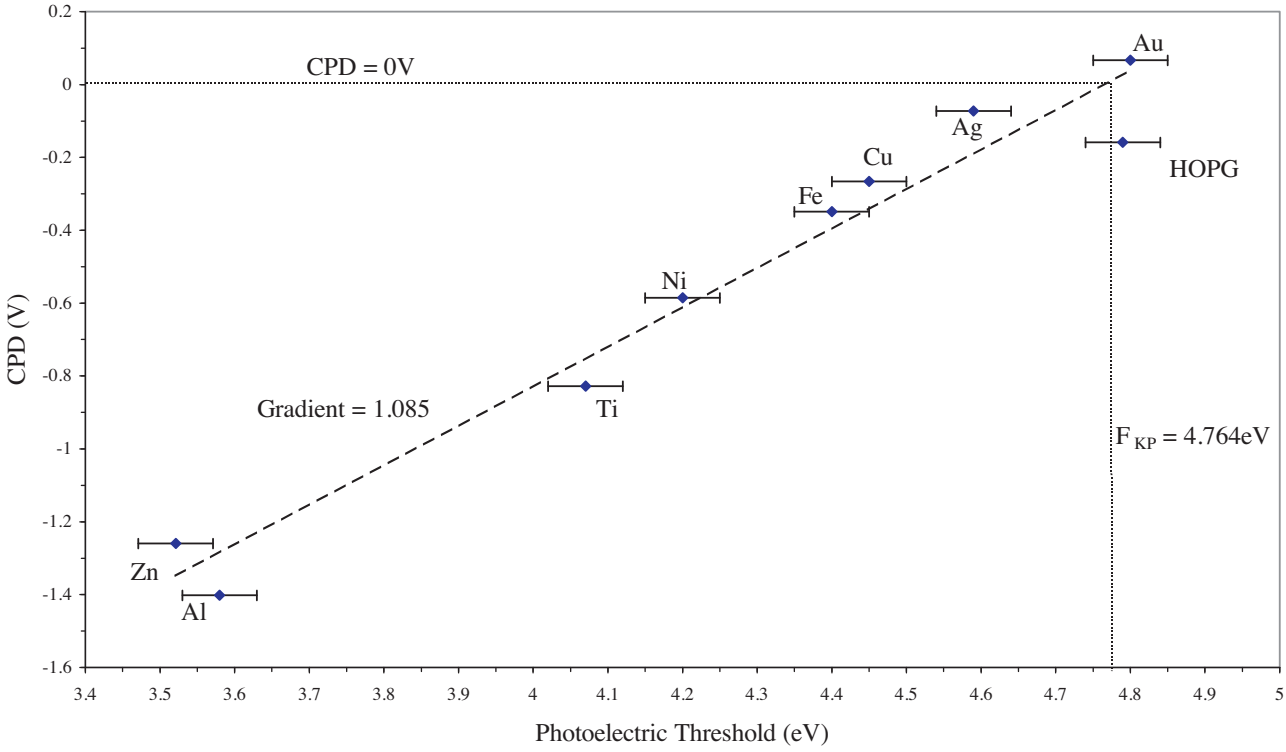


**Fig. 11.** Plot of CPD in volts versus initial photoelectric threshold (eV) for Al, Zn, Ti, Ni, Fe, Cu, Ag, Au metals and HOPG. The sample data lie line on a line of near unity gradient ($m$ = 1.085). The KP tip absolute work function of 4.764 eV is determined for the position CPD = 0. Error bars in the photoelectric threshold plot are ± 0.5 eV, the $V_{cpd}$ error is approximately 0.003 V.

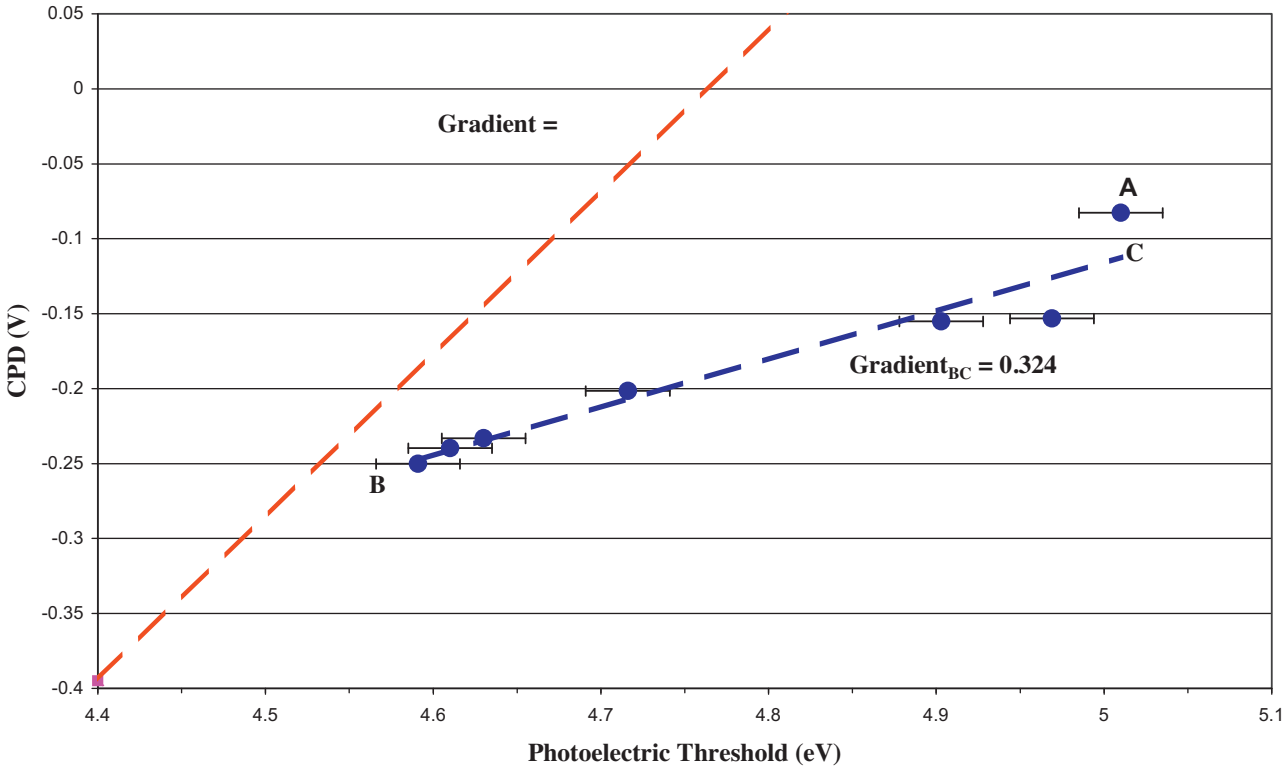


**Fig. 12.** Variation of CPD (dark) and initial photoelectric threshold over a 24 h period after surface cleaning of a second well-oxidized Cu surface in ambient. Point A represents a Cu sample with native oxide layer due to exposure to ambient for several days. Point B represents a newly cleaned Cu surface, Line BC is the oxidation process followed for 24 h after cleaning. The Cu oxidation curve (blue line) has a much lower gradient (0.324) than the metal line (Gradient 1.085), shown on Fig. 11, most probably due to the formation of a semiconductor energy gap. The copper oxide surface displays a white light sensitivity (Surface Photovoltage) of some 70 meV. (For interpretation of the references to color in this figure legend, the reader is referred to the web version of this article.)

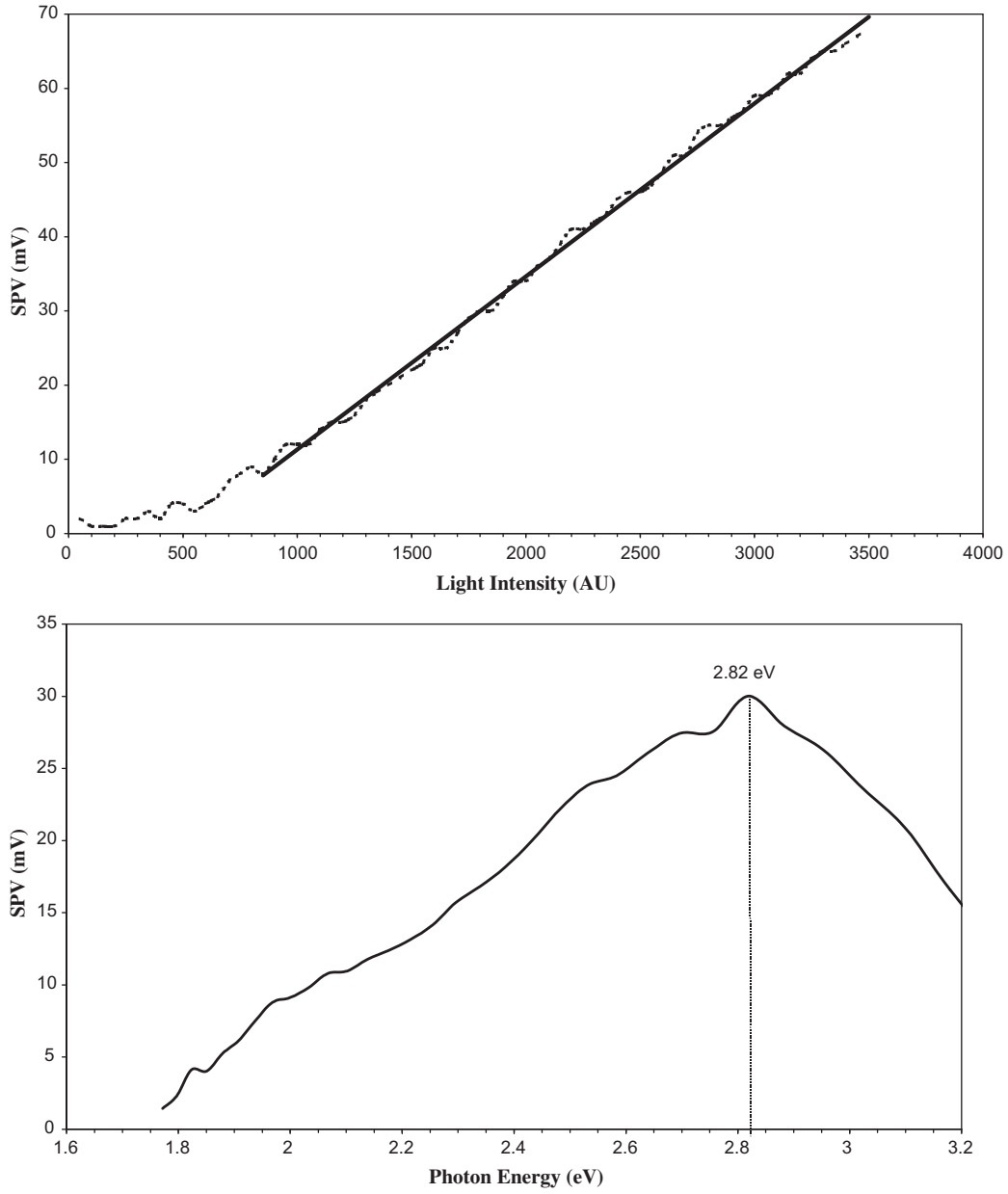


**Fig. 13.** Top SPV response versus white light intensity for a well-oxidized copper surface, bottom maxima in the SPS occur at 2.82 eV.

**Table 1**
Sample absolute work functions, literature and CPD values.

| Sample | Photoelectric threshold (eV) | WF lit (eV) | CPD (V) |
|---|---|---|---|
| Ag | 4.59 | 4.73 [17] | −0.072 |
| Al | 3.58 | 3.60 [18] | −1.4017 |
| Au | 4.80 | 4.82 [17] | 0.0663 |
| Cu | 4.45 | 4.45 [18] | −0.2654 |
| Fe | 4.40 | 4.34 [17] | −0.3492 |
| HOPG | 4.79 | 4.80 [19] | −0.159 |
| Ni | 4.2 | 4.25 [18] | −0.5851 |
| Ti | 4.07 | 4.06 [17] | −0.8276 |
| Zn | 3.52 | 3.63 [20] | −1.274 |

ambient and vacuum conditions (on atomically clean surfaces) is required to fully explore the range of $\Phi$'s reported in the literature.

In Fig. 12 we show the result of cleaning a *second* Cu sample. Point "A" represents a surface that has been oxidized for several days, and line BC the loci of ($V_{cpd}$, photoemission threshold) formed over 24 h after cleaning. We observe the gradient of this line is quite different from the original "metal" line, it is much smaller. We observed a visible light sensitivity of the Cu surface, suggesting initial formation of a semiconductor oxide. The reduced gradient of the ($V_{cpd}$, photoemission threshold) line "BC" compared to that the various metals shown in Fig. 10. indicates $\Delta V_{cpd} < \Delta\Phi$. Fig. 13

### 3.4. Surface photovoltage spectroscopy of copper oxide

We have investigated the electronic properties of the Cu oxide surface using a second tuneable visible light source, spectrometer 2 in Fig. 4. Fig. 11 (top) shows the white light intensity-dependent SPV of some 70 meV and the associated SPS scan (1.8–3.2 eV) produces a maximum at 2.82 eV indicating the onset of the band-gap response producing a non-equilibrium SCR [13]. The reported maxima is close to the 2.4 eV optical band-gap reported for $Cu_2O$ [22] and the copper surface colour (red) further supports this conclusion. Our results can be interpreted, in electron energy diagram terms, as the cleaned metal Fermi-level migrating to a conduction

band–valence band, with band-gap $E_g$. During oxidation the $E_f$ shift is approx. −0.10 to−0.15 V. The substantially larger change in the initial photoemission threshold of approx. 0.450 eV indicates that the valance band edge is moving to lower energies, coupled with the onset of a band-gap. Recently Roy and Gopinath [23] have used a helium I source and $K\alpha$ XPS core spectra to study the oxidation of polycrystalline copper surfaces at pressures of 0.3 mBar. At 300 K they report broad Cu 3d features at 2–4 eV and 7–8.5 eV above $E_f$ in the He I binding energy spectra and O 2p features at 1.3 and 2–6 eV in the XPS–VB spectra. They attribute a shift of 0.6 eV to a work function change.

## 4. Conclusion

We have presented a new ambient pressure photoemission technique based upon a Kelvin probe detector which generates information on the initial photoelectric threshold and the contact potential difference $V_{cpd}$ of metal substrates and HOPG. We have overcome the limitation of inelastic scattering of photoejected electrons by air molecules by rastering the irradiation energy of the DUV photons rather than employing a retarding-field analysis as in conventional UPS. The S/N ratio of the photoresponse R from Au, Ag, Cu, Fe, Ni, Ti, Zn, Al and HOPG was high. As predicted by Fowler Theory, above the photoemission threshold we observe straight-line segments in the intensity-corrected $R^{1/2}$ data. The $V_{cpd}$ versus initial photoelectric threshold exhibit a near unity gradient. Illumination of an oxidized copper surface by a second tuneable visible source (QTH) produced a SPV of circa 70 mV and a corresponding peak in the SPS response at 2.84 eV, close to the reported optical bandgap of $Cu_2O$. We have followed the copper oxidation process in ambient and show that ($V_{cpd}$, photoemission threshold) loci gradient is less than unity. We interpret this as evidence of formation of a semiconductor bandgap and consequently the photoemission threshold energy increases as the semiconductor valance band forms.

Ambient pressure photoemission employs low energy photons close to $E_F$ and is unlikely to damage surfaces. This system has potential applications in characterizing surfaces, interfaces, TCO's and indeed operational electronic devices such as solar cells. There is no impediment in operating at ambient, reduced pressure or indeed under vacuum conditions.

## References

[1] I.D. Baikie, P.J. Estrup, Low cost PC based scanning Kelvin probe, Rev. Sci. Instrum. 69 (1998) 3902–3997.
[2] I.D. Baikie, U. Petermann, A. Speakman, B. Lägel, K. Dirscherl, P.J. Estrup, Work function study of rhenium oxidation using an ultra high vacuum scanning Kelvin probe, J. Appl. Phys. 88 (2000) 4371–4376.
[3] U. Petermann, I.D. Baikie, B. Lägel, K.M. Dirscherl, Work functions of polycrystalline metals using UHV SKP, Mater. Res. Soc. Symp. 615 (6.6) (2000) 1–6.
[4] I.D. Baikie, U. Petermann, B. Lägel, In-situ work function study of oxidation and thin film growth on clean surfaces, Surf. Sci. 433–435 (1999) 770–774.
[5] K. Dirscherl, I.D. Baikie, G. Forsyth, A. van der Heide, Utilisation of a micro-tip scanning Kelvin probe for non-invasive surface potential mapping of mc-Si solar cells, Sol. Energy Mater. Sol. Cells 70 (2003) 485–494.
[6] Y. Lee, J. Wang, J.W.P. Hsu, Surface photovoltage characterization of organic photovoltaic devices, Appl. Phys. Lett. 103 (2013) 173302–173312.
[7] P. Pingel, D. Neher, Comprehensive picture of p-type doping of P3HT with the molecular acceptor F4TCNQ, Phys. Rev. B: Condens. Matter 87 (2013) 115209.
[8] Y. Lin, J. Zeng, Tuning the work function of graphene by ultraviolet irradiation, Appl. Phys. Lett. 102 (2013) 183120.
[9] T. Aytun, A. Turak, D. Baikie, G. Halek, C.W. Ow-Yan, Solution processed LiF for work function tuning in electrode bilayers, Nano Lett. 12 (2012) 39–44.
[10] I.D. Baikie, U. Peterman, B. Lagel, K. Dirscherl, Study of high- and low-work-function surfaces for hyperthermal surface ionization using an absolute Kelvin probe, J. Vac. Sci. Technol. A19 (2001) 1460–1466.
[11] N.D. Orf, I.D. Baikie, O. Shapira, Y. Fink, Work function engineering in low-temperature metals, Appl. Phys. Lett. 94 (2009) 113504–113506.
[12] J.S. Kim, B. Lägel, E. Moons, N. Johansson, I.D. Baikie, W.R. Salaneck, R.H. Friend, F. Cacialli, Kelvin probe and ultraviolet photoemission measurements of indium tin oxide work function: a comparison, Synth. Met. 111–112 (2000) 311–314.
[13] L. Kronik, Y. Shapira, Surface photovoltage spectroscopy of semiconductor structures: at the crossraods of physics, chemistry and electrical engineering, Surf. Int. Anal. 31 (9) (2001) 954–965.
[14] M.P. Seah, W.A. Dench, Quantitative electron spectroscopy of surfaces: a standard database for electron inelastic mean free paths in solids, Surf. Interfaces Anal. 1 (1979) 2–11.
[15] R.H. Fowler, The analysis of photoelectric sensitivity curves for clean metals at various temperatures, Phys. Rev. 38 (1931) 45.
[16] C.R. Crowell, J.C. Sarace, S. Sze, Tungsten-semiconductor Schottky-barrier diodes, Trans. Met. Soc. AIME 233 (1965) 478.
[17] E.A. Mechtly, in: Mac E. Van (Ed.), "Properties of Materials" in Reference Data for Engineers: Radio, Electronics, Computer and Communications, Butterworth-Heinemann, Valkenburg, 2002, pp. 4-1–4-33.
[18] M. Uda, Open counter for low energy electron detection, Jpn. J. Appl. Phys. 24 (1985) 284.
[19] A. Sherehiy, S. Dumpala, A. Safir, D. Mudd, I. Arnold, R.W. Cohn, M.K. Sunkara, G.U. Sumanasekera, Thermionic Emission Properties and The Work Function Determination of Arrays of Conical Carbon Nanotubes, Dia. and Relat. Mater. 34 (2013) 1–8.
[20] J. Holzl, F.K. Schulte, Springer Tracts Mod. Phys. 85 (1979) 1.
[21] D.E. Eastman, Photoelectric work functions of transition, rare-earth and noble metals, Phys. Rev. B: Condens. Matter 2 (1970) 1.
[22] M. Johan, M. Suan, N. Hawari, H.A. Ching, Annealing effects on the properties of copper oxide thin films prepared by chemical deposition, Int. J. Electrochem. Sci. 6 (2011) 6094.
[23] K. Roy, C.S. Gopinath, UV photoelectron spectroscopy at near ambeint pressures: mapping valance band electronic structure changes from Cu to CuO, Anal. Chem. 86 (2014) 3683–3687.